A Learnable Optimization and Regularization Approach to Massive MIMO CSI Feedback

Zhengyang Hu, Guanzhang Liu, Qi Xie, Jiang Xue, *Senior Member, IEEE*,
Deyu Meng, *Member, IEEE*, and Deniz Gündüz, *Fellow, IEEE*

***Abstract*—Channel state information (CSI) plays a critical role in achieving the potential benefits of massive multiple input multiple output (MIMO) systems. In frequency division duplex (FDD) massive MIMO systems, the base station (BS) relies on sustained and accurate CSI feedback from users. However, due to the large number of antennas and users being served in massive MIMO systems, feedback overhead can become a bottleneck. In this paper, we propose a model-driven deep learning method for CSI feedback, called learnable optimization and regularization algorithm (LORA). Instead of using l_1-norm as the regularization term, LORA introduces a learnable regularization module that adapts to characteristics of CSI automatically. The conventional Iterative Shrinkage-Thresholding Algorithm (ISTA) is unfolded into a neural network, which can learn both the optimization process and the regularization term by end-to-end training. We show that LORA improves the CSI feedback accuracy and speed. Besides, a novel learnable quantization method and the corresponding training scheme are proposed, and it is shown that LORA can operate successfully at different bit rates, providing flexibility in terms of the CSI feedback overhead. Various realistic scenarios are considered to demonstrate the effectiveness and robustness of LORA through numerical simulations.**

***Index Terms*—Massive MIMO; CSI feedback; model-driven; deep learning; regularization learning.**

I. Introduction

As a core technology for the sixth generation (6G) of wireless networks, massive multiple input multiple output (MIMO) systems can provide higher data rates and link reliability [1]. To realize the benefits provided by massive MIMO systems, such as beamforming [2] and more reliable signal detection [3], accurate channel state information (CSI) at the base station (BS) is necessary in both the time division duplex (TDD) and frequency division duplex (FDD) modes. In the TDD mode, downlink CSI can be obtained directly from uplink CSI under the assumption of perfect channel reciprocity. However, the TDD mode may not work well in time sensitive scenarios, such as live streaming and vehicular communications [4]. In the FDD mode, the uplink and downlink use different frequency resources at the same time. However, due to the lack of perfect channel reciprocity in the FDD mode, user equipments (UEs) need to estimate downlink CSI and feed it back to the BS [5]. Nevertheless, the huge feedback overhead due to the large number of antennas at the BS and the large number of users being served can become a significant performance bottleneck. Therefore, a CSI feedback method with low overhead and high accuracy is essential to deliver the promised gains of massive MIMO systems in next generation communication networks.

Due to the strong spatial correlations and the shared local scatterers in the propagation environment in massive MIMO systems, CSI exhibits approximate sparsity in the angular-delay domain, which means that CSI matrix can be compressed significantly to reduce the feedback overhead [6]. Compressive sensing (CS)-based methods can be used to project sparse signals to a low-dimensional space and recover them efficiently with theoretical guarantees. The first CS-based CSI feedback method for massive MIMO systems was proposed in [7], which considered both two dimensional-discrete Fourier transformation (2D-DFT) and Karhunen-Loeve Transform (KLT) as sparsifying bases. In [8], the authors used the statistical information about the angle-of-departure (AOD) to develop a basis for sparsity mapping and a weighted l_1-norm was proposed for recovery, which was shown to achieve a better performance than the DFT basis. Considering orthogonal frequency-division multiplexing (OFDM) systems, a multidimensional CS-based analog CSI feedback method was proposed in [9], which treated the CSI feedback design as a multidimensional matrix compression and recovery problem, and exploited the tensor decomposition method. However, these methods are limited in general as they cannot identify the best basis, and the projected CSI matrices are often not perfectly sparse, resulting in performance loss. Although some particular priors are shown to reduce the strict requirement of sparsity [8], [10], [11], these 'manual' designs are done in a case-by-case basis and are still not efficient enough due to the diverse use cases and high performance requirements of future systems.

In recent years, data-driven methods, in particular, deep learning (DL), has achieved notable success in a variety of wireless communication applications [12], such as channel estimation [13], signal detection [3], joint source-channel coding [14], channel prediction [15], and beamforming [16]. Besides, DL-based methods have also made tremendous strides in

The work of Jiang Xue and Zhengyang Hu were supported by the National Key R&D Program of China under Grant 2020YFA0713900 and in part by the Joint Project of Industries and Universities Shaanxi under Grant S2021-YF-GXZD 0076. The work of Qi Xie was supported in part by the China NSFC Project under contracts 62206214. The work of Deyu Meng was supported by the Macao Science and Technology Development Fund under Grant 061/2020/A2, and the China NSFC projects under contract 61721002.

Zhengyang Hu, Guanzhang Liu, Qi Xie, Jiang Xue and Deyu Meng are with School of Mathematics and Statistics, Xi'an Jiaotong University, Xi'an, 710049, China (e-mail: hzyxjtu@stu.xjtu.edu.cn, lgzh97@stu.xjtu.edu.cn, xie.qi@xjtu.edu.cn, x.jiang@xjtu.edu.cn and dymeng@mail.xjtu.edu.cn).

Deniz Gündüz is with the Department of Electrical and Electronic Engineering, Imperial College London, London SW7 2AZ, U.K. (e-mail: d.gunduz@imperial.ac.uk).

The corresponding author is Jiang Xue.

increasing the quality of CSI feedback [17].

The authors in [18] were the first to employ DL for CSI feedback reduction and proposed a simple convolutional neural network (CNN) auto-encoder architecture for dimensionality reduction, which has been considered as a baseline for the follow-up studies on DL-based CSI feedback methods. The encoder and decoder in [18] carry out the compression and recovery operations, respectively. Since increasing the receptive field in CNN can extract more information from the input, CsiNet+ in [19] considers different convolution kernel dimensions. Inspired by the inception model, the authors in [20] designed CRNet, which used multi-paths and multi-receptive fields in both encoder and decoder to improve the performance. MRFNet proposed in [21] shows that the larger number of convolution channels can recover more details of CSI. The authors in [22] exploited the dilate convolution operator to increase the receptive field without increasing the number of parameters, while retaining a high performance. In [23], the popular self-attention architecture, named transformer, was exploited for CSI feedback. To design the lightweight neural network (NN) for CSI feedback, the authors in [24] exploited the complex-value convolution operator and proposed a X-shape NN architecture to reduce the complexity of the NN. In [25], the NNs for real and imaginary parts share parameters, which reduces the complexity of the NN. In [26], projected CSI coefficients are further quantized, and entropy coded to reduce the required rate, and a significant improvement was reported with respect to CsiNet [18]. This approach was extended to CSI feedback from multiple nearby users in [27], where the correlation among CSI matrices was taken in to account to achieve better compression efficiency. Researchers have also adopted other DL techniques for CSI feedback. The authors in [28] proposed a CSI feedback method based on generative adversarial networks (GANs). In [29], CSI feedback is modeled as an image super resolution problem, and SRNet is proposed. In [30], inspired by the elastic network, ACRNet is proposed to adjust the complexity and performance of the NN. To extract time correlation of CSI, CNN-LSTM-A [31] and CsiNet-LSTM [32] are proposed. Feedback schemes that are designed for a particular task, such as beamforming, were investigated in [33], [34], which could reduce the feedback overhead by bypassing channel estimation. Although the aforementioned CNN-based methods have achieved significant performance improvements compared to their CS-based counterparts, these methods simply treat the channel matrix as a two-dimensional 'image' with local correlations, which may limit their performance.

Model-driven DL methods exploit our prior knowledge about the particular learning problem. Bringing model-driven and data-driven approaches together, model-driven DL methods not only make the learned model more explainable and predictable [35], but also avoid the requirements for accurate and explicit modeling. In [36], the authors proposed a model-driven DL method to improve the recovery accuracy in CSI feedback, by unfolding a conventional CS algorithm into a NN and learning the measurement matrix. Inspired by the transformation matrix design and unfolding, TiLISTA-Joint was proposed in [37], which not only learned the down-sampling matrix, but also used a sparse auto-encoder architecture to learn the sparse transformation. To further improve the recovery accuracy, the authors exploited the attention mechanism for learning sparse transformation and proposed FISTA-Net in [38]. In [39], the authors designed a model-driven module to pre-compress CSI based on self-information, and the entire NN was trained in a data-driven manner. For the better presentation and easier reading, we present TABLE I to summarize and show the detailed technical information of related works. Key ideas and main characteristics show the similarities and differences of these works, respectively.

Although model-driven DL methods have exhibited remarkable success in CSI feedback, current methods are all designed with an l_1-norm regularization term, which cannot extract the prior knowledge of CSI in some cases. Actually, how to design a suitable regularization (i.e., data prior) is an active research problem in machine learning. It is well-known that l_0-norm is the optimal regularization term to describe sparsity, but the optimization with l_0-norm is untractable. When the measurement matrix satisfies restricted isometry property (RIP) condition, l_1-norm is equivalent to l_0-norm in terms of sparse signal recovery [43]. The authors in [44] utilized a mixture of Gaussian distributions to learn the noise distribution. Although the proposed method in [44] does not explicitly formulate a regularization term, the data prior is learned through the loss function. Due to the strength of DL, the authors proposed a proximal dehaze-net, which learned a haze-related prior to achieve the obvious performance gain in single photo dehazing [45]. In [46], the authors proposed RCDNet to automatically extract the prior from rain images for better deraining.

Inspired by the model-driven methods for CSI feedback and regularization term learning in [44]–[46], in this paper, we propose a joint regularization and optimization method, called learnable optimization and regularization algorithm (LORA). LORA exploits a NN to learn the regularization term for better fitting the characteristics of CSI, and develops an iterative algorithm with learnable parameters to achieve performance gains.

The main contributions of this work are summarized as follows:

- Existing model-driven DL architectures for CSI feedback all unfold the algorithm derived from an optimization problem with the l_1-norm regularization term, which cannot describe the prior of CSI well due to its imperfect sparsity. Instead, LORA treats the regularization term as a learnable function that can be adjusted according to the characteristics of CSI itself. The proposed method results in a novel algorithm of model-driven DL for CSI feedback with significant improvements in the performance in terms of both the normalized mean square error (NMSE) and the achievable average rate.
- To further mitigate the effect of quantization in LORA, we exploit quantization-aware training (QAT) with learnable quantization parameters, such as quantization scale and zero point value. The proposed quantization method eases the performance decay caused by quantization in

TABLE I: Summary of key ideas and main characteristics of related works.

Key ideas	Related works	Main characteristics
Convolution operator design	CsiNet+ [19]	Increasing the depth and width of the CsiNet
	CRNet [20]	Strip convolution kernel pattern, multiple paths and feature fusion
	MRFNet [21]	Large number of convolution channels
	DCRNet [22]	Increasing receptive fields with dilated convolution
Novel DL techniques	TransNet [23]	Self-attention and transformer
	[28]	GAN
	SRNet [29]	Image super resolution technique
	ACRNet [30]	Elastic network and network aggregation technique
Multi-domain correlation utilization	Distributed DeepCMC [27]	Correlation among nearby users' CSI
	CNNLSTM-A [31]	Correlation among the time domain with the attention mechanism
	CSINET-LSTM [32]	Correlation among the time domain based on CsiNet
Joint other modules	[33]	Joint the channel estimation, CSI feedback and beamforming
	[34]	Joint the channel estimation, CSI feedback and beamforming with multiple users, and exploiting users correlations
Model-driven DL methods	[36]	Learning the measurement matrix
	TiLISTA-Joint [37]	Learning the measurement matrix, step size, sparse auto-encoder and sparse transformation
	FISTA-Net [38]	Unfolding FISTA and considering both sparsity and low-rank properties of CSI
	IdasNet [39]	Using a model-driven module to pre-compress CSI based on the self-information
Changeable compression rate	[40]	Designing an overhead control unit to discard part of the output of the encoder
	[41]	Using principal component analysis to compress CSI and proposing a quantization method based on k-means clustering
Viewing CSI as sequence	[42]	Regarding CSI as a sequence and proposing a novel network based on 2D-LSTM

different bit levels.

- The numerical results show that LORA has a superior performance than CsiNet+ [19], CRNet [20], DCRNet [22], TransNet [23], ACRNet [30], TiLISTA-Joint [37] and ISTA-NET in different scenarios based on 3GPP TR 38.901 [47]. Moreover, the performance with channel estimation error and complexity comparisons are provided. We also carry out ablation studies to explore the effects of different modules of LORA on the final performance.

The rest of this work is organized as follows. Section II describes the massive MIMO system, CSI feedback procedure and channel model. We re-formulate the CSI feedback problem and present the basic algorithm in Section III. In Section IV, we present LORA with insights in detail. Numerical results and analyses are provided in Section V to demonstrate the superiority of LORA compared to the existing CSI feedback schemes. Finally, the paper is concluded in Section VI.

Notations: Throughout the paper, bold uppercase letters, bold lowercase letters and non-bold letters are used to denote matrices, vectors and scalars, respectively. $\|\cdot\|_2$ is the Euclidean norm. $|\cdot|$ stands for element-wise absolute value. $(\cdot)^T$ and $(\cdot)^H$ are transpose and conjugate transpose, respectively. The real and complex number fields are $\mathbb{R}$ and $\mathbb{C}$, respectively. The expectation operation is represented by $\mathbb{E}\{\cdot\}$. $\triangleq$ is used to indicate the definition of the value and new variable, while $\simeq$ represents approximate equality. $\mathcal{CN}(\mu_g, \sigma_g^2)$ denotes complex Gaussian distribution with mean μ_g and variance σ_g^2.

II. System Model

A. Massive MIMO system and DL-based CSI feedback

We consider the downlink of a single-cell massive MIMO OFDM system in the FDD mode, where a BS equipped with $N_t \gg 1$ antennas serves a single-antenna user equipment (UE) [18] over $\tilde{N}_c$ subcarriers. The received signal at the n-th subcarrier $(n = 1, \ldots, \tilde{N}_c)$ in the frequency domain can be expressed as

$$y_n = \tilde{\boldsymbol{h}}_n^H \boldsymbol{v}_n x_n + z_n, \tag{1}$$

where $\tilde{\boldsymbol{h}}_n \in \mathbb{C}^{N_t \times 1}$, $\boldsymbol{v}_n \in \mathbb{C}^{N_t \times 1}$ and $x_n \in \mathbb{C}$ are the downlink channel vector, corresponding precoding vector and the modulated transmitted signal, respectively, while $z_n \sim \mathcal{CN}(0, 1)$ denotes the complex random additive Gaussian noise. The detailed channel model will be introduced in Section II-B. In the FDD mode, the downlink channel vector $\tilde{\boldsymbol{h}}_n$ has to be estimated at the UE and sent back to the BS. The overall downlink CSI matrix can be expressed as $\tilde{\boldsymbol{H}} = [\tilde{\boldsymbol{h}}_1, \tilde{\boldsymbol{h}}_2, \cdots, \tilde{\boldsymbol{h}}_{\tilde{N}_c}] \in \mathbb{C}^{N_t \times \tilde{N}_c}$, which consists of $2N_t\tilde{N}_c$ real numbers after decomposing the complex matrix into real and imaginary parts. $\tilde{\boldsymbol{H}}$ can be transformed from the spatial-frequency domain to the angular-delay domain by a 2D-DFT as

$$\boldsymbol{H}_f = \boldsymbol{F}_d \tilde{\boldsymbol{H}} \boldsymbol{F}_a, \tag{2}$$

where $\boldsymbol{F}_d \in \mathbb{C}^{N_t \times N_t}$ and $\boldsymbol{F}_a \in \mathbb{C}^{\tilde{N}_c \times \tilde{N}_c}$ are the DFT matrices. As mentioned, $\boldsymbol{H}_f$ has approximate sparsity in the angular-delay domain. Moreover, only the first[1] few columns of $\boldsymbol{H}_f$ have significant values because the delay between multipath components typically lies within a limited period in the delay domain. So, we preserve only the first $N_c < \tilde{N}_c$ columns and remove the rest. An example illustrating the real part of the complete and cropped channel matrices in the angular-delay domain, and the complete channel matrix in the spatial-frequency domain are shown in Fig. 1. We denote the truncated CSI matrix by $\boldsymbol{H}$, which consists of $2N_tN_c$ real numbers after decomposing the real and imaginary parts. Although the required number of feedback parameters has been reduced

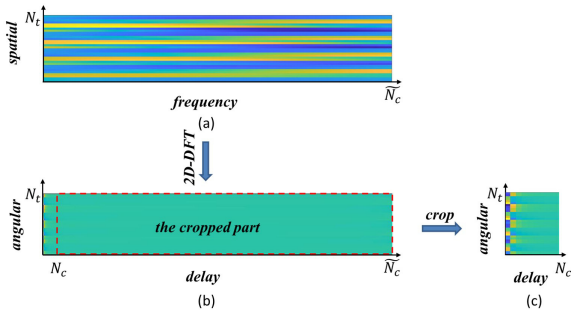

Fig. 1: The real part of the complete channel matrix in (a) spatial-frequency domain, the real part of the complete (b) and the cropped (c) channel matrices in angular-delay domain.

[1]The exact subset of significant values depends on the distribution of the channel, and does not always correspond to the first part.

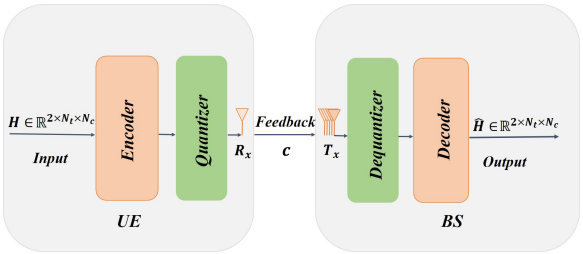

Fig. 2: CSI feedback procedure.

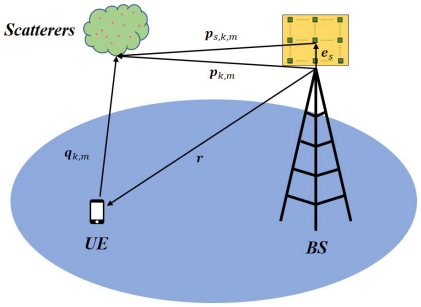

Fig. 3: The geometric relationship between the BS, UE and scatterers.

from $2N_t \times \tilde{N}_c$ to $2N_t \times N_c$, the feedback overhead is still too large and will consume significant channel resources.

Following the prior works, we consider a pair of encoder-decoder networks to compress and recover CSI, and a pair of quantizer-dequantizer to reduce the required CSI feedback bits. As shown in Fig. 2, $\boldsymbol{H} \in \mathbb{R}^{2\times N_t\times N_c}$ is fed into the encoder network, whose output is M floating point parameters. Then, these parameters are quantized to a bit stream by the quantizer, whose output is denoted by $\boldsymbol{c}$. The dequantizer and the decoder are applied at the BS. The dequantizer transforms $\boldsymbol{c}$ back to floating point numbers, and the decoder transforms the dequantizer output to $\hat{\boldsymbol{H}} \in \mathbb{R}^{2\times N_t\times N_c}$. The compression ratio (CR) is defined as CR $\triangleq M/2N_tN_c$. The whole feedback procedure can be presented as

$$\boldsymbol{c} = \mathcal{Q}_e\left(f_e(\boldsymbol{H}, \Theta_e), \Theta_q\right), \tag{3}$$

$$\hat{\boldsymbol{H}} = f_d\left(\mathcal{Q}_d\left(\boldsymbol{c}, \Theta_{dq}\right), \Theta_d\right), \tag{4}$$

where $\hat{\boldsymbol{H}}$ is the reconstructed and cropped CSI, f_e and f_d denote the encoder and decoder functions, $\mathcal{Q}_e$ and $\mathcal{Q}_d$ denote the quantizer and dequantizer functions, while Θ_e, Θ_d, Θ_q, Θ_{dq} are the parameters of f_e, f_d, $\mathcal{Q}_e$ and $\mathcal{Q}_d$, respectively. The complete CSI can be obtained by zero-padding followed by inverse DFT operation on $\hat{\boldsymbol{H}}$.

B. Channel model

Due to the large size of the antenna array in massive MIMO systems, spherical wave channel model should be considered instead of a plane wave channel model [48]. This is also verified through measurements in [49] and [50]. Spherical wave channel model is more realistic, and has been widely adopted in wireless communication applications [51]–[53]. We also adopt a 3-D geometric stochastic channel model [54] in this work, which incorporates the spherical wave channel model.

We model the paths and sub-paths of channels distinctly by considering the scatterers in the environment. The adopted model does not require an exact geometric representation of the environment, but instead, relies on the statistical distribution of the scattering clusters. The last-bounce scatterers in the single-bounce[2] model is considered, which focus on the signal propagation from the last scatterers to the receiver, and is not an exact geometric representation of the propagation environment. The locations of the last-bounce scatterers are used to generate the channel coefficients. The length of the k-th path, d_k, can be expressed as

$$d_k = \|\boldsymbol{r}\|_2 + \tau_k c, \tag{5}$$

where $\|\boldsymbol{r}\|_2$ is the distance between the BS and the UE, τ_k is the delay of the k-th path, and c is the speed of light. We define $\boldsymbol{q}_{k,m}$ as the arrival vector of the m-th sub-path in the k-th path pointing from the UE location to the scatterers. Then, its length can be expressed as

$$\|\boldsymbol{q}_{k,m}\|_2 = \frac{d_k^2 - \|\boldsymbol{r}\|_2^2}{2(d_k + \boldsymbol{r}^T \bar{\boldsymbol{q}}_{k,m})}, \tag{6}$$

where

$$\bar{\boldsymbol{q}}_{k,m} \triangleq \begin{bmatrix} \cos\phi_{k,m}^a \cos\theta_{k,m}^a \\ \sin\phi_{k,m}^a \cos\theta_{k,m}^a \\ \sin\theta_{k,m}^a \end{bmatrix}, \tag{7}$$

$\phi_{k,m}^a$ and $\theta_{k,m}^a$ are the azimuth and elevation angle of arrival (AOA) of the m-th sub-path in the k-th path, respectively. The location of the scatterers can be obtained by the geometric relationship shown in Fig. 3.

To model the spherical wave, each antenna element s at the BS is considered separately. Given an reference antenna (which can be chosen arbitrarily in the antenna array) element location and its departure vector of the m-th sub-path in the k-th path $\boldsymbol{p}_{k,m}$, the departure vector of the s-th antenna of the m-th sub-path in the k-th path $\boldsymbol{p}_{s,k,m}$, the corresponding elevation AOD $\theta_{s,k,m}^d$ and azimuth AOD $\phi_{s,k,m}^d$, can be derived as

$$\theta_{s,k,m}^d = \arcsin\frac{p_{s,k,m,z}}{\|\boldsymbol{p}_{s,k,m}\|_2}, \tag{8}$$

and

$$\phi_{s,k,m}^d = \arctan\frac{p_{s,k,m,y}}{p_{s,k,m,x}}, \tag{9}$$

where

$$\boldsymbol{p}_{s,k,m} = \boldsymbol{p}_{k,m} - \boldsymbol{e}_s, \tag{10}$$

and $\boldsymbol{e}_s$ is the vector from the reference antenna element to the s-th antenna element, while $p_{s,k,m,x}$, $p_{s,k,m,y}$ and $p_{s,k,m,z}$ are the Cartesian coordinate components of $\boldsymbol{p}_{s,k,m}$. Therefore, the deterministic phase $\psi_{s,k,m}$ and delay $\tau_{s,k}$ can be derived by

$$\psi_{s,k,m} = \frac{2\pi}{\lambda_c}(d_{s,k,m} \bmod \lambda_c), \tag{11}$$

[2]The following illustrations are based on the single-bounce model for simplifying notations, which can be easily extended to the multi-bounce model. In Section V, the proposed method is evaluated on the multi-bounce model. More details about the multi-bounce model can be found in [54].

and

$$\tau_{s,k} = \frac{\sum_{m=1}^{M_k} d_{s,k,m}}{M_k c}, \tag{12}$$

where

$$d_{s,k,m} = \|\boldsymbol{p}_{s,k,m}\|_2 + \|\boldsymbol{q}_{k,m}\|_2, \tag{13}$$

M_k is the number of sub-paths in the k-th path, λ_c is the wavelength, and mod stands for the modulo operation. Therefore, the channel between the s-th BS antenna and the UE via the k-th path can be described as (14), where $\boldsymbol{P}_{s,k,m}$, $F_{\mathrm{rx},\theta}$, $F_{\mathrm{rx},\varphi}$, $F_{\mathrm{tx},\theta}$, $F_{\mathrm{tx},\varphi}$, j and $\psi_{k,m}^0$ are the polarization coupling matrix of the s-th antenna of the m-th sub-path in the k-th path, elevation polarimetric antenna response at the receiver, azimuth polarimetric antenna response at the receiver, elevation polarimetric antenna response at the transmitter, azimuth polarimetric antenna response at the transmitter, imaginary unit, and the random phase of the m-th sub-path in the k-th path, respectively.

Therefore, the (s,l)-th element of $\tilde{\boldsymbol{H}}$ in spatial-frequency domain can be expressed as

$$\tilde{\boldsymbol{H}}_{s,l} = \sum_{k=1}^{K'} g_{s,k} e^{\left(-j2\pi \frac{l-1}{\tilde{N}_c} B' \tau_{s,k}\right)}, \tag{15}$$

where B' is the bandwidth, K' is the number of paths, $s = 1, \cdots, N_t$ and $l = 1, \cdots, \tilde{N}_c$.

III. Problem Formulation

In this section, we first formulate CSI feedback as a linear inverse problem. Then, the iterative shrinkage-thresholding algorithm (ISTA) will be introduced, which inspired the proposed method.

A. Problem formulation

We consider a learnable matrix as the encoder, which can be conveniently designed as a light linear layer, and is appropriate for the UE due to its limited computation and storage ability. Therefore, the projected vector $\boldsymbol{v}$ can be expressed as

$$\boldsymbol{v} = \boldsymbol{A}\boldsymbol{x}, \tag{16}$$

where $\boldsymbol{A}$ is the learnable matrix and $\boldsymbol{x} \in \mathbb{R}^{2N_t N_c}$ is the CSI matrix $\boldsymbol{H}$ in the vector form. Then, the decoder at the BS can be regarded as solving an inverse problem, which is presented as

$$\min_{\boldsymbol{x}} \frac{1}{2}\|\boldsymbol{v} - \boldsymbol{A}\boldsymbol{x}\|_2^2. \tag{17}$$

Due to the huge dimension reduction, the problem (17) is highly ill-posed; and hence, hard to solve directly. Typically, a regularization term is introduced into the optimization function to exploit any known prior information about the optimal solution. Therefore, the problem (17) can be modified as

$$\min_{\boldsymbol{x}} \frac{1}{2}\|\boldsymbol{v} - \boldsymbol{A}\boldsymbol{x}\|_2^2 + R(\boldsymbol{x}), \tag{18}$$

where $R(\boldsymbol{x})$ is the regularization term.

B. ISTA

Considering the sparsity of CSI, conventional CS-based and model-driven DL methods utilize l_1-norm as the regularization term. Then, the problem (18) can be written as

$$\min_{\boldsymbol{x}} \frac{1}{2}\|\boldsymbol{v} - \boldsymbol{A}\boldsymbol{x}\|_2^2 + \lambda\|\boldsymbol{x}\|_1. \tag{19}$$

ISTA [55] is a classical iterative method to solve (19), and the related model-driven DL methods for CSI feedback [36], [37] are inspired by it. Its iterative formulation at the t-th step can be expressed as follows:

$$\boldsymbol{u}^{(t)} = \boldsymbol{x}^{(t-1)} - \alpha \boldsymbol{A}^T \left(\boldsymbol{A}\boldsymbol{x}^{(t-1)} - \boldsymbol{v}\right), \tag{20}$$

$$\boldsymbol{x}^{(t)} = \mathrm{sign}(\boldsymbol{u}^{(t)})\max(\boldsymbol{0}, |\boldsymbol{u}^{(t)}| - \boldsymbol{\theta}), \tag{21}$$

where $\boldsymbol{u}^{(t)}$, $\boldsymbol{0}$, $\boldsymbol{\theta}$ and α are the intermediate variable, zero vector, thresholding term and step size, respectively. The sign and $\max$ are element-wise operations, which can be expressed as

$$\mathrm{sign}(u) = \begin{cases} 1 & \text{if } u > 0, \\ 0 & \text{if } u = 0, \\ -1 & \text{otherwise}, \end{cases} \tag{22}$$

and

$$\max(u, \theta) = \begin{cases} u & \text{if } u \geq \theta, \\ \theta & \text{if } u < \theta. \end{cases} \tag{23}$$

IV. Design of LORA and Training Scheme

In this section, we first propose a novel model-driven DL method, called LORA, which unfolds the derived iterative formulations to a NN and incorporates a regularization learning module. Moreover, considering the quantization in CSI feedback procedure, QAT and learnable quantization methods will be employed.

A. Architecture of LORA

As in Equation (16) presented above, we consider the CSI in the vector form. However, instead of fixing the regularization term to l_1-norm, we consider $R(\boldsymbol{x})$ as a learnable transform, which is assumed to be differentiable. Then, the iterative formulation at the t-th step ($t = 1, \ldots, T$) in the solution of problem (18) can be derived as

$$\boldsymbol{x}^{(t)} = \boldsymbol{x}^{(t-1)} - \alpha^{(t-1)} \Big(\boldsymbol{A}^T(\boldsymbol{A}\boldsymbol{x}^{(t-1)} - \boldsymbol{v}) + \nabla R(\boldsymbol{x}^{(t-1)})\Big), \tag{24}$$

where $\nabla R(\cdot)$ stands for the gradient of $R(\cdot)$. Built upon the idea of unfolding, the decoder of LORA is developed by treating each iteration as a separate layer, which are connected sequentially. The step size α in (24) is set as a learnable parameter that is different in each layer. The matrix $\boldsymbol{A}$ is the same one used by the encoder. Different from the previous works designing the sparsity transformation to fit a fixed regularization term, we employ a learnable regularization term to better fit the characteristics of CSI, and learn the regularization term implicitly. To learn $\nabla R(\cdot)$, each layer employs a regularization learning module, which will be introduced in detail in the next sub-section. Together with the encoder,

$$g_{s,k} = \sum_{m=1}^{M_k} \begin{bmatrix} F_{\mathrm{rx},\theta}\left(\theta^a_{k,m}, \varphi^a_{k,m}\right) \\ F_{\mathrm{rx},\varphi}\left(\theta^a_{k,m}, \varphi^a_{k,m}\right) \end{bmatrix}^T \boldsymbol{P}_{s,k,m} \begin{bmatrix} F_{\mathrm{tx},\theta}\left(\theta^d_{s,k,m}, \varphi^d_{s,k,m}\right) \\ F_{\mathrm{tx},\varphi}\left(\theta^d_{s,k,m}, \varphi^d_{s,k,m}\right) \end{bmatrix} e^{\left(-j\psi^0_{k,m} - j\psi_{s,k,m}\right)} \tag{14}$$

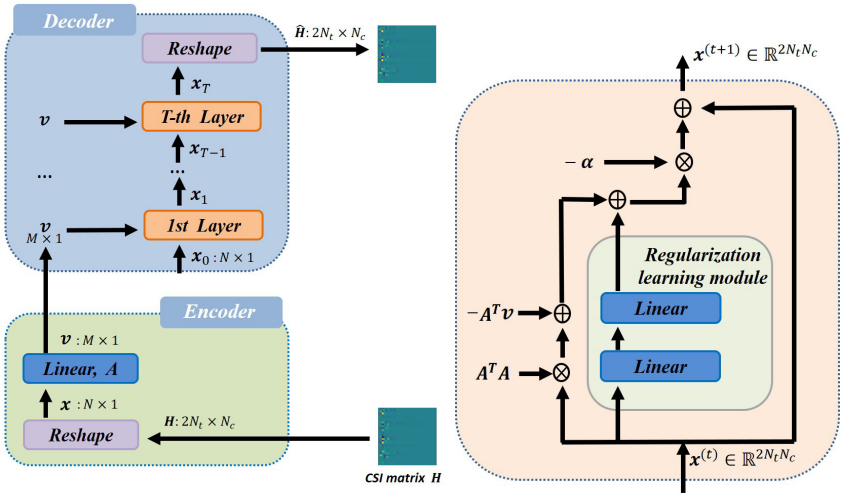

Fig. 4: The NN architecture and forward procedure of LORA: (a) shows the overall architecture of LORA for the encoder and decoder, (b) shows the detailed architecture of a single layer of the LORA decoder, including the regularization learning module.

a complete NN architecture is established, and the overall architecture of LORA is presented in Fig. 4 (a).

Model-driven DL exploits NNs to replace explicit expressions or manually set parameters in model-based iterative algorithms. This can mitigate the performance loss due to inaccurate modeling, while exploiting the valuable knowledge of the model simultaneously. Besides, model-driven DL methods can also prevent the over-fitting problem, and are usually easier to train compared to purely data-driven NN approaches.

Notably, the initialization of $\boldsymbol{x}$ is important due to the use of gradient descent. Since CSI has sparsity, and its values are near zero, $\boldsymbol{x}^{(0)} = \mathbf{0}$ is considered as the initialization for LORA.

B. Regularization learning module

The parameters in ISTA, such as the measurement matrix, step size, etc, are all treated as learnable parameters in existing works. However, the regularization term is set as conventional l_1-norm. Meanwhile, l_1-norm is not a fully accurate prior because of the weak sparsity of CSI. Even with strict sparsity, the measurement matrix needs to satisfy RIP condition to ensure the exact signal recovery by using l_1-norm. Therefore, making the regularization learnable to directly fit the characteristics of CSI is a promising approach.

The architecture of the regularization learning module is shown in Fig. 4 (b), which is a light multi-layer perceptron (MLP). The number of neurons of the input layer, hidden layer, and output layer of the regularization learning module are set as $2N_tN_c$, N_m and $2N_tN_c$, respectively. Therefore, the mathematical expression for the regularization learning module can be expressed as

$$\mathrm{MLP}(\mathbf{x}) = \boldsymbol{W_2}\sigma\left(\boldsymbol{W_1}\mathbf{x}\right), \tag{25}$$

where $\boldsymbol{W_1} \in \mathbb{R}^{N_m \times 2N_tN_c}$ and $\boldsymbol{W_2} \in \mathbb{R}^{2N_tN_c \times N_m}$ are the parameters of the first and second linear layers, $\sigma(\cdot)$ is the rectified linear unit (ReLU) activation function and $\mathbf{x} \in \mathbb{R}^{2N_tN_c}$ is the input.

The reasons for choosing MLP as the architecture of the regularization learning module are as follows: (1) MLP has the universal approximation property [56], and hence, it is capable to characterize the complex properties of CSI; (2) The linear layer in MLP has a dense connection architecture, which can keep the original information as much as possible compared to a locally connected architecture, such as a convolution operator. Since the regularization term is part of the optimization problem, which is fixed once the training is finished, the parameters of the MLP should be shared by all the layers. This also reduces the number of trainable parameters.

C. Training scheme with quantization

LORA is trained in an end-to-end manner. Mean square error (MSE) is used as the loss function, which can be written as

$$L(\Theta) = \frac{1}{\mathcal{T}} \sum_{i=1}^{\mathcal{T}} \|\hat{\boldsymbol{H}}_i - \boldsymbol{H}_i\|_2^2, \tag{26}$$

where $\mathcal{T}$ is the total number of samples in the training set and Θ denotes the parameters of the NN, including the MLP. To avoid hyper-parameter tuning for dynamic learning rate

adjustment operator, ADAM [57] with fixed learning rate is applied as the optimization operator.

The quantization module is also considered in CSI feedback for practical implementation. The conventional quantization procedure can be written as

$$\mathsf{q} = \mathrm{round}\left(\mathrm{clip}\left(\frac{\mathsf{r}-\mathsf{z}}{\mathsf{s}}, \mathsf{n}, \mathsf{p}\right)\right), \tag{27}$$

$$\mathsf{b} = \mathrm{num2bit}(\mathsf{q}), \tag{28}$$

where r refers to real number to be quantized, s and z are the scale and zero point values, respectively (i.e., the parameters of the quantization function), q is an integer corresponding to the quantized value, $\mathrm{num2bit}$ is the function that converts an integer to its binary representation, b is the resultant bit stream, $\mathsf{n} = -2^{B-1}$ and $\mathsf{p} = 2^{B-1}-1$ are the lower and upper bounds on the clip function, B is the number of quantization bits per real dimension, round is the rounding function that maps a floating number to the closest integer, clip function aims to limit the range of the input, which can be expressed as

$$\mathrm{clip}(x, \mathsf{n}, \mathsf{p}) = \begin{cases} \mathsf{n} & \text{if } x < \mathsf{n}, \\ x & \text{if } \mathsf{n} \le x \le \mathsf{p}, \\ \mathsf{p} & \text{if } x > \mathsf{p}. \end{cases} \tag{29}$$

The corresponding dequantization procedure can be expressed as

$$\bar{\mathsf{q}} = \mathrm{bit2num}(\mathsf{b}), \tag{30}$$

$$\hat{\mathsf{r}} = \bar{\mathsf{q}} \times \mathsf{s} + \mathsf{z}, \tag{31}$$

where $\mathrm{bit2num}$ is the function which converts a binary number b to the equivalent integer value, $\bar{\mathsf{q}}$, and $\hat{\mathsf{r}}$ is the dequantized float values corresponding to r. Quantization and dequantization operations can be regarded as two blocks, which are inserted to the end of the encoder and the beginning of the decoder, respectively. Therefore, the forward procedure of NN can be regarded as CSI feedback with quantization and dequantization. Meanwhile, since end-to-end training is applied, the backward procedure can be regarded as learning the parameters with the effect of quantization. However, the rounding function is not differentiable, which would prevent back-propagation during training. Instead, we can employ straight-through differentiation [58], where we set

$$\frac{\partial \mathrm{round}(x)}{\partial x} \triangleq 1. \tag{32}$$

The aforementioned training scheme is a modified QAT method, which is inspired by the QAT in NN quantization [59]. Although QAT achieves a reasonable performance, it still has the weakness that the scale and zero point values are manually set. As the quantization procedure is embedded into the end-to-end training, the scale and zero point values can also be learned and trained jointly. Considering back-propagation during training, the derivatives of scale and zero point values can be derived from (27), (31) and (32) as follows:

$$\begin{aligned} \frac{\partial \hat{\mathsf{r}}}{\partial \mathsf{s}} &= \frac{\partial \bar{\mathsf{q}}}{\partial \mathsf{s}}\mathsf{s} + \bar{\mathsf{q}} \\ &\simeq \frac{\partial\left(\frac{\mathsf{r}-\mathsf{z}}{\mathsf{s}}\right)}{\partial \mathsf{s}}\mathsf{s} + \bar{\mathsf{q}} \\ &\simeq \begin{cases} -\frac{\mathsf{r}-\mathsf{z}}{\mathsf{s}} + \mathrm{round}(\frac{\mathsf{r}-\mathsf{z}}{\mathsf{s}}) & \text{if } \mathsf{n} < \frac{\mathsf{r}-\mathsf{z}}{\mathsf{s}} < \mathsf{p} \\ \mathsf{n} \quad \text{or} \quad \mathsf{p} & \text{otherwise,} \end{cases} \end{aligned} \tag{33}$$

$$\begin{aligned} \frac{\partial \hat{\mathsf{r}}}{\partial \mathsf{z}} &= \frac{\partial \bar{\mathsf{q}}}{\partial \mathsf{z}}\mathsf{s} + 1 \\ &\simeq \frac{\partial\left(\frac{\mathsf{r}-\mathsf{z}}{\mathsf{s}}\right)}{\partial \mathsf{z}}\mathsf{s} + 1 \\ &\simeq \begin{cases} 0 & \text{if } \mathsf{n} < \frac{\mathsf{r}-\mathsf{z}}{\mathsf{s}} < \mathsf{p} \\ 1 & \text{otherwise,} \end{cases} \end{aligned} \tag{34}$$

where the derivatives of $\mathrm{clip}(x, \mathsf{n}, \mathsf{p})$ at $x = \mathsf{n}$ and $x = \mathsf{p}$ are set as 0 [60].

We name the scale learnable quantization method as LSQ, and both scale and zero point value learnable quantization method as LSZQ. The LSQ and LSZQ are modified versions of the NN quantization methods in [61] and [60], respectively.

V. Numerical Experiment

In this section, we study the effects of different design options of LORA. We present numerical results evaluating the performance of LORA in terms of the reconstruction accuracy, and the achievable rate.

A. Experiment settings

1) Data generation: QuaDRiGa [54] is a general channel simulator that meets the 3GPP standards. The spherical waves introduced in Section II as well as other realistic scenarios can be modeled by QuaDRiGa. Therefore, in this work, we use QuaDRiGa to generate CSI matrices in rural macro non-line-of-sight (RMANLOS), urban macro non-line-of-sight (UMANLOS), and urban micro non-line-of-sight (UMINLOS) scenarios. The carrier frequency, number of subcarriers, subcarrier interval, and N_c are set as 3.5GHz, 1024, 30kHz and 32, respectively, for the above three scenarios. The BS is equipped with a cross-polarized uniform planar array (UPA) with half wavelength antenna spacing, where the number of horizontal antennas is 4, and the number of vertical antennas is 4 and 8 for $N_t = 32$ and $N_t = 64$, respectively. The UE is assumed to move along a linear trajectory with a velocity of $\hat{v}$ = 6km/h. The heights of the BS are 10m, 10m, and 25m for the RMANLOS, UMINLOS and UMANLOS scenarios, respectively. Training and test datasets are generated with 40000 and 10000 samples, respectively.

2) Training settings and evaluation metric: LORA is implemented in PyTorch. The parameters of the NN are updated and optimized by the ADAM optimizer with default settings. The learning rate, number of epochs and batch size are set to 0.001, 1000 and 200, respectively. The number of layers in LORA, i.e., T, is set as 4, while N_m is set as 1024 in the simulations. We use the NMSE as the evaluation metric, which is defined as

$$\mathrm{NMSE} \triangleq \mathbb{E}\left\{\frac{\|\boldsymbol{H} - \hat{\boldsymbol{H}}\|_2^2}{\|\boldsymbol{H}\|_2^2}\right\}. \tag{35}$$

TABLE II: The NMSE performance of the output of each layer of a trained LORA using MLP and CNN for CR$=1/16$ in the RMANLOS scenario.

Order of Layers	MLP	CNN
1	**0.2936**	0.317
2	**0.0888**	0.5911
3	**0.0174**	0.0848
4	**0.0012**	0.0753

Unless stated otherwise, all experiments are implemented with the above settings.

B. Ablation studies for the LORA architecture

In this sub-section, the effects of different design options of LORA will be studied. The design motivations presented in Section IV are supported by the following results.

1) Architecture of the regularization learning module: To further motivate using MLP as the regularization learning module, we present the output of the last layer using MLP and CNN[3] in Fig. 5. The part of the output of the last layer, which corresponds to the real part of the CSI, is shown in the figure. By comparing the visualization results, it can be seen that using CNN loses some information in the region of red box, while the MLP recovers them well. To further investigate the effect of two architectures to the iterative optimization procedure, we also calculate the NMSE of the output of each layer in LORA, which is given in TABLE II. It can be seen that MLP has better performances than CNN at all iterations. The above visualization and numerical results show that using MLP for the regularization learning module in LORA achieves a better performance than using CNN.

2) Effect of the learnable regularization module: To verify the effectiveness of the regularization learning module in LORA, and to motivate the particular architecture argued for in Section IV-A, the performance of conventional ISTA[4], ISTA-NET, TiLISTA-Joint and LORA are compared next. The ISTA-NET stands for an ISTA unfolding method, which has learnable measurement matrix, step size and threshold. In TiLISTA-Joint, in addition to the parameters in ISTA-NET, a sparse transformation is also learned. In this experiment, the conventional ISTA is the baseline method, which has no learnable part. The results are shown in Fig. 6. As we can see, the performance increases as we learn more parameters of the underlying model. This phenomenon suggests that the performance can be improved by making more of the model parameters learnable. Specifically, the results verify that the learnable regularization outperforms fixing l_1-norm as the regularization term. In addition, the importance of regularization in terms of the performance can be shown among the compared DL methods.

We also compare the l_1-norm of the output of the ISTA-NET and LORA, to further study the learned regularization term. The results are shown in TABLE III. Although the learned regularization term has no explicit formulation, we can conclude that the learned regularization term is different from the conventional l_1-norm, and the improved performance of LORA with the learned regularization term confirms that l_1-norm is not the right regularization for this problem.

TABLE III: l_1-norm of the output of different methods for CR$=1/16$ in the UMANLOS and UMINLOS scenarios.

Method \ Scenario	UMANLOS	UMINLOS
ISTA-NET	3.74	8.18
LORA (ours)	4.39	10.15

TABLE IV: The NMSE performance of LORA with different number of layers and width of MLP for CR$=1/64$ in the RMANLOS scenario.

Number of Neurons (N_m) \ Number of Layers (T)	4	5	6	7
512	0.1791	0.1706	0.1656	0.1625
1024	0.0099	0.0071	0.0055	0.0047
4096	0.1629	0.0137	0.0105	0.0081

3) Effect of different layers of LORA and the width of MLP: The number of layers of LORA and the width of the hidden layer in MLP are investigated next. The impact of these two hyper-parameters on the performance of LORA can be seen in TABLE IV. If the performance is more important and the increased complexity can be accommodated, such as the high accuracy communication, LORA has the potential to improve the performance by using more layers according to the results in TABLE IV. We also observe that increasing the width of MLP from $N_m = 512$ to $N_m = 1024$ can significantly boost the performance. Indeed, simply using a wider MLP can be sufficient as the gains from increasing the number of layers from $T = 4$ to $T = 7$ is relatively marginal in this case. Moreover, it is worth mentioning that increasing the width or depth of a NN can make training process more difficult, e.g., due to gradient vanishing and explosion. In TABLE IV, we can observe that increasing N_m from 1024 to 4096 results in a worse NMSE performance. To maximize the performance in each setting, the training parameters, such as the learning rate and batch size, need to be carefully adjusted.

C. Further performance results

In this sub-section, the performance of LORA is evaluated in the aforementioned three scenarios, and compared with seven benchmarks to investigate its effectiveness and robustness. CsiNet+ [19] and CRNet [20] are considered as two CNN-based benchmarks. Meanwhile, TiLISTA-Joint [37] and the ISTA-NET are considered as the unfolding-based benchmarks. To further highlight the superiority of LORA, DCRNet [22], TransNet [23] and ACRNet [30] are also applied as benchmarks. The results are shown in Fig. 7 - Fig. 9 for the three scenarios RMANLOS, UMANLOS and UMINLOS, respectively. LORA outperforms all benchmarks clearly for all CR values in all the scenarios, especially for small CR values. The presented results demonstrate the superiority of LORA compared to recent works in terms of the recovery accuracy

[3]The CNN here consists of two convolutional layers with a ReLU activation function. The convolution filter sizes are 3×3 and the numbers of convolution channels in the two layers are 32 and 2, respectively.

[4]We choose Gaussian matrix as the measurement matrix.

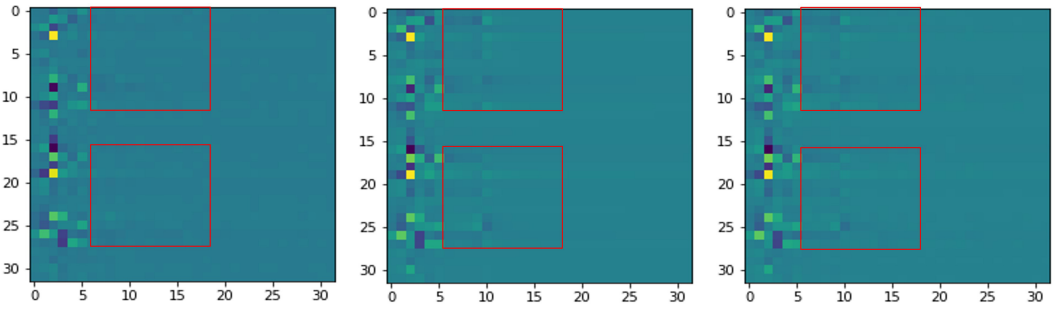

(a) (b) (c)

Fig. 5: The visualization of the real part of the CSI from the last layer of a trained LORA with (a) CNN and (b) MLP as two alternative architectures for the regularization learning module, while (c) is the groundtruth. The significant differences are marked by red boxes.

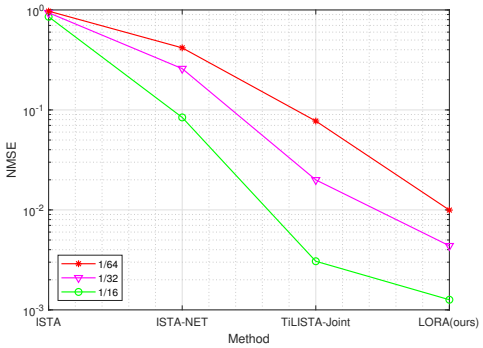

Fig. 6: The NMSE performance of different ISTA-based methods for different CR values in the RMANLOS scenario.

TABLE V: The NMSE performance of the proposed method in RMANLOS scenario with a 64-antenna BS serving UEs with 2 antennas.

CR	1/16	1/32	1/64
NMSE	0.00031	0.00347	0.01062

even for CR $= 1/64$. Moreover, the robustness of LORA in terms of achieving a superior performance in a variety of communication scenarios and CR values are verified. We conclude that LORA is a promising method for practical cases with high performance and small overhead. Next, we consider a more complex scenario with a 64-antenna BS serving UEs with 2 antennas. The NMSE performance of the proposed method in this scenario is presented in TABLE V. The results show that the proposed method can be easily extended to more antennas at the UEs or the BS, and serve more complex massive MIMO systems.

Next, to evaluate the robustness of LORA against channel estimation errors, we study its performance with imperfect CSI. In particular, different from the above experiments that assumed perfect CSI at the UE, an additive white Gaussian noise is added to the CSI during both training and testing stages. The NMSE performance for CR$= 1/64$ of TiLISTA-Joint and LORA in the RMANLOS scenario are compared. The signal-to-noise ratio (SNR) of CSI is used to adjust the

TABLE VI: The number of parameters of different methods in the encoder and decoder, respectively.

Method	CR=1/4		CR=1/64	
	Encoder	Decoder	Encoder	Decoder
CsiNet+	1,048,772	1,069,936	65,732	86,896
TiLISTA-Joint	1,048,576	11,468,820	65,536	10,485,780
LORA(ours)	1,048,576	16,777,220	65,536	16,777,220

noise level introduced to the CSI. According to the results in Fig. 10, LORA significantly outperforms TiLISTA-Joint in all imperfect CSI noise levels, which suggests that LORA has better capability to adapt to different degrees of channel estimation errors. Notably, the NMSE here is defined as

$$\text{NMSE} \triangleq \mathbb{E}\left\{\frac{\|\boldsymbol{H}_{gt}-\hat{\boldsymbol{H}}\|_2^2}{\|\boldsymbol{H}_{gt}\|_2^2}\right\}, \tag{36}$$

where $\boldsymbol{H}_{gt}$ denotes the perfect CSI. Since the input of LORA contains channel estimation errors, the results in Fig. 10 also show the denoising capability of LORA in addition to the CSI compression and recovery.

D. Complexity

Here, we analyze the storage and computational complexity of LORA. At the encoder of LORA, there is only a measurement matrix, which has $\left((2N_tN_c)^2 \times \text{CR}\right)$ parameters. At the decoder of LORA, each layer has a learning rate parameter and a regularization learning module, which has $(4N_tN_c \times N_m)$ parameters. Thus, the total number of parameters of LORA is $((2M + 4TN_m) \times N_tN_c + T)$. Thanks to parameter sharing among regularization learning modules of different layers, the number of trainable parameters of LORA can be reduced to $((2M + 4N_m)N_tN_c + T)$. The number of parameters of CsiNet+, TiLISTA-Joint and LORA at the encoder and decoder are also shown in TABLE VI for both CR$= 1/4$ and CR$= 1/64$. The results show that unfolding-based methods have slightly fewer parameters at the encoder, but significantly more parameters are needed at the decoder. It is because the convolution operator in CsiNet+ shares parameters and has less connections with the output of the former layer than MLP. However, since the BS usually has large storage, it is desirable to employ a larger model on the decoder side.

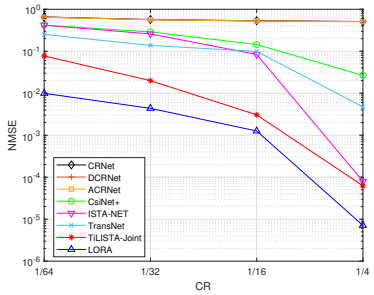

Fig. 7: The NMSE performance versus CR for different methods in the RMANLOS scenario.

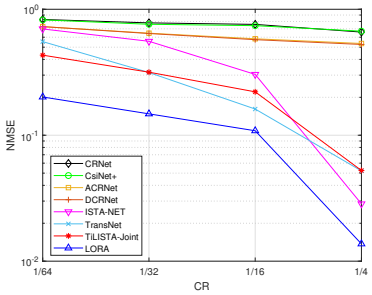

Fig. 8: The NMSE performance versus CR for different methods in the UMANLOS scenario.

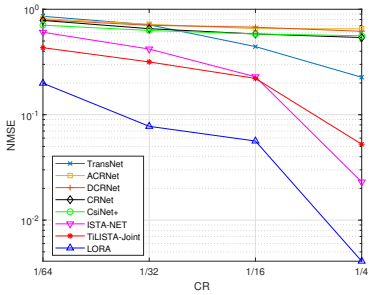

Fig. 9: The NMSE performance versus CR for different methods in the UMINLOS scenario.

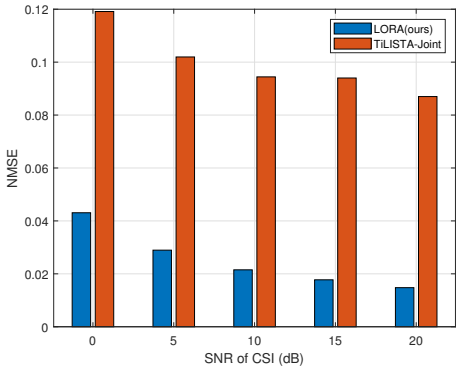

Fig. 10: The NMSE performance with different SNRs.

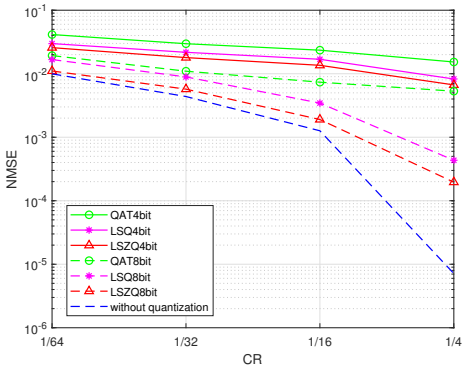

Fig. 11: The NMSE performance versus CR for different quantization methods and bit levels in the RMANLOS scenario.

TABLE VII: The computation costs of different methods for CR$=1/64$ in the RMANLOS scenario.

Method	Training time (sec.)	Test time (sec.)
ISTA	-	90.96
CsiNet+	64.307	6.712
TiLISTA-Joint	109.688	10.432
LORA(ours)	**29.337**	**3.54**

The main operator employed in LORA is a linear layer, whose computational cost can be calculated as $N_{in} \times N_{out}$, where N_{in} and N_{out} are the sizes of the input and output of the linear layer, respectively. Therefore, the encoder, decoder and total computational complexity of LORA are $\mathcal{O}(MN_cN_t)$, $\mathcal{O}(TMN_t^2N_c^2)$ and $\mathcal{O}(TMN_t^2N_c^2)$, which indicates that the computational cost of LORA depends on the number of layers, antennas, preserved sub-carriers and feedback parameters. In the following, CR$=1/64$ is used as an example to compare the running time of one epoch of three DL-based methods, and the training and test times are shown in seconds (sec.) in TABLE VII. According to TABLE VII, it is obvious that LORA costs the least time among the compared methods, which shows the superiority of LORA in terms of computing time. Comparing the LORA results with these of ISTA and TiLISTA-Joint, we conclude that introducing the learnable regularization term improves the recovery performance while reducing the inference time. It can be clearly observed that DL-based methods have faster inference speed. Although the proposed method will cost extra time in training compared with conventional ISTA, which does not require any training at all, training be done offline and online fine-tuning or MAML [62] methods can be exploited to reduce the cost of training in non-stationary environments.

E. Quantization

In the above simulations, we ignored the quantization error. In this sub-section, the proposed quantization method is evaluated. We first compare jointly training LORA and the quantizer-dequantizer parameters with training the quantizer-dequantizer on a well-trained LORA. The NMSE of these two approaches are 0.0053 and 0.0069, respectively, for CR$=1/4$ in the RMANLOS scenario. Hence, as one would expect, joint training is preferable as the NN parameters adapt to the quantization effect. We next compare three methods for four different CR values and two different bit levels in the RMANLOS scenario. The NMSE performance of the quantization methods are presented in Fig. 11. QAT is the baseline method for comparison, while the dashed line without marks refers to LORA without quantization. It can be seen that LSQ and LSZQ both outperform QAT. Moreover, the performance increases with the number of learnable parameters in the quantization module; that is LSZQ outperforms LSQ. Comparison with LORA without quantization benchmark shows that quantization decreases the performance of LORA, especially when the number of quantization bits is small. The results not

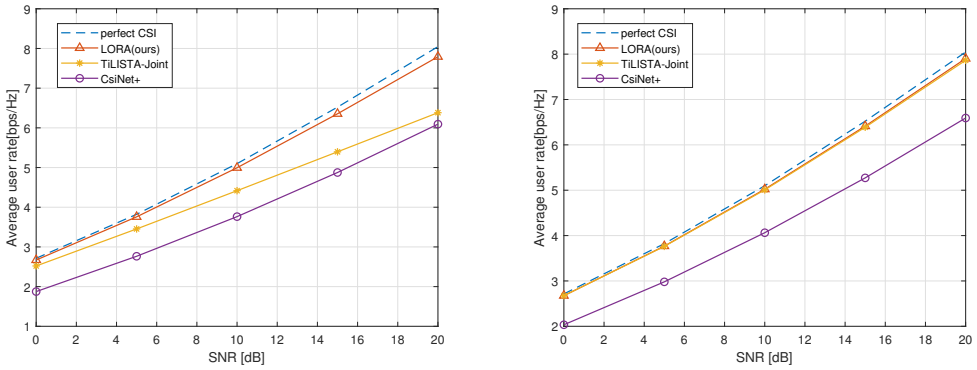

(a) CR= $1/64$ (b) CR= $1/4$

Fig. 12: The achievable rate versus SNR for (a) CR= $1/64$ and (b) CR= $1/4$ in the UMANLOS scenario.

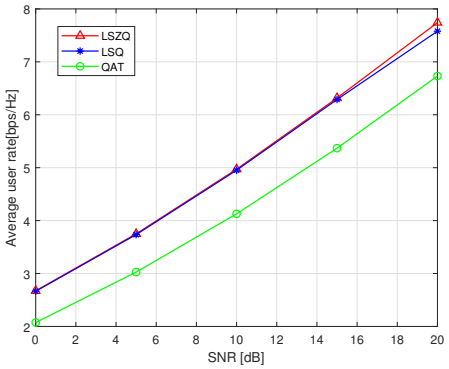

Fig. 13: The achievable rate versus SNR with 4-bit quantization with different methods in the RMANLOS scenario.

only verify that the scale and zero point value are essential parameters of the quantization, but also demonstrate the effectiveness of making these parameters learnable. As expected, the performance of all three methods improve with the number of quantization bits. In addition, the performance of LSQ and LSZQ increase with the increase in CR more significantly in 8-bit quantization than 4-bit quantization. It is also interesting that the improvement of LSQ and LSZQ compared to QAT also increases with the number of quantization bits. This phenomenon may be attributed to the fact that the impacts of scale and zero point parameters are amplified due to the increase in the number of quantization bits.

F. Communication performance analysis

So far, we have mainly analyzed the NMSE performance of LORA. However, in practical systems, the goal of providing accurate CSI feedback is to improve the communication performance. Hence, in this section, we consider the average achievable user rate to evaluate the performance, where zero-forcing (ZF) is used as the precoding algorithm. ZF is applied independently for all sub-carriers to calculate the corresponding rates, and the results are averaged over the number of sub-carriers. The details of how these rates are evaulated can be found in [63] and [64]. We generate 8000 samples for training and 2000 samples for the test. The number of sub-carriers is set to 512, while the other variables remain the same as in Section V-A.

The performance of TiLISTA-Joint, CsiNet+, and the proposed LORA method versus SNR for CR= $1/64$ and CR= $1/4$ in the UMANLOS scenario are shown in Fig. 12 (a) and Fig. 12 (b), respectively. The dotted line represents the achievable rate with perfect CSI knowledge, which can be regarded as an upper bound. From the figure, it can be seen that the proposed method outperforms the compared methods for both CR values, while the improvement with respect to TiLISTA-Joint is more significant in the high compression case. Moreover, the gaps between LORA and the upper bound are uniformly narrow across all SNRs for both CR= $1/64$ and CR= $1/4$. Since the overhead is large for CR= $1/4$, the gap between LORA and TiLISTA-Joint is small, and both of which perform close to the upper bound. The achievable average rate results corroborate the comparisons based on the NMSE, and verify the superiority of LORA.

To further verify the effectiveness of the proposed quantization method, we evaluate the rate performance of the three quantization methods considered in Fig. 11. According to the results presented in Fig. 13, the quantization methods with learnable parameters outperform the method without learnable parameters, also in terms of the rate performance. We also observe that the gap between the rates achieved by the LSQ and LSZQ is rather small, which may attribute to the fact that the rate is a logarithmic function of the SNR, which shrinks the relatively larger gap observed in terms of the NMSE.

VI. Conclusion

In this paper, a model-driven DL method, called LORA, has been proposed for efficient CSI feedback in FDD massive MIMO systems. LORA is constructed by unfolding an iterative optimization algorithm with learnable parameters. Specifically, the derivative of the regularization term of the optimization problem is parameterized as a MLP to automatically and directly extract the characteristics of CSI instead of using the fixed conventional l_1-norm. Besides, a scale and zero

point value learnable quantization method with the end-to-end training was proposed to ease the performance decay caused by quantization. Numerical results not only show effects of various components of LORA, supporting the presented architecture, but also demonstrate the superiority and robustness of this architecture with respect to existing techniques in the literature. It has been also shown that LORA with the proposed quantization method can be effective at different bit levels, providing flexibility in terms of the available feedback channel capacity.

REFERENCES

[1] F. Rusek, D. Persson, B. K. Lau, E. G. Larsson, T. L. Marzetta, O. Edfors, and F. Tufvesson, "Scaling up MIMO: Opportunities and challenges with very large arrays," *IEEE Signal Processing Magazine*, vol. 30, no. 1, pp. 40–60, 2013.

[2] S. Lakshminarayana, M. Assaad, and M. Debbah, "Coordinated multicell beamforming for massive MIMO: A random matrix approach," *IEEE Transactions on Information Theory*, vol. 61, no. 6, pp. 3387–3412, 2015.

[3] J. Sun, Y. Zhang, J. Xue, and Z. Xu, "Learning to search for MIMO detection," *IEEE Transactions on Wireless Communications*, vol. 19, no. 11, pp. 7571–7584, 2020.

[4] S. Ji and M. Li, "CLNet: Complex input lightweight neural network designed for massive MIMO CSI feedback," *IEEE Wireless Communications Letters*, vol. 10, no. 10, pp. 2318–2322, 2021.

[5] M. S. Sim, J. Park, C.-B. Chae, and R. W. Heath, "Compressed channel feedback for correlated massive MIMO systems," *Journal of Communications and Networks*, vol. 18, no. 1, pp. 95–104, 2016.

[6] Z. Gao, L. Dai, S. Han, C.-L. I, Z. Wang, and L. Hanzo, "Compressive sensing techniques for next-generation wireless communications," *IEEE Wireless Communications*, vol. 25, no. 3, pp. 144–153, 2018.

[7] P. Kuo, H. T. Kung, and P. Ting, "Compressive sensing based channel feedback protocols for spatially-correlated massive antenna arrays," in *2012 IEEE Wireless Communications and Networking Conference (WCNC)*, 2012, pp. 492–497.

[8] L. Lu, G. Y. Li, D. Qiao, and W. Han, "Sparsity-enhancing basis for compressive sensing based channel feedback in massive MIMO systems," in *2015 IEEE Global Communications Conference (GLOBECOM)*, 2015, pp. 1–6.

[9] P. Cheng and Z. Chen, "Multidimensional compressive sensing based analog CSI feedback for massive MIMO-OFDM systems," in *2014 IEEE 80th Vehicular Technology Conference (VTC2014-Fall)*, 2014, pp. 1–6.

[10] C. A. Metzler, A. Maleki, and R. G. Baraniuk, "From denoising to compressed sensing," *IEEE Transactions on Information Theory*, vol. 62, no. 9, pp. 5117–5144, 2016.

[11] X. Rao and V. K. N. Lau, "Distributed compressive CSIT estimation and feedback for FDD multi-user massive MIMO systems," *IEEE Transactions on Signal Processing*, vol. 62, no. 12, pp. 3261–3271, 2014.

[12] D. Gündüz, P. de Kerret, N. D. Sidiropoulos, D. Gesbert, C. R. Murthy, and M. van der Schaar, "Machine learning in the air," *IEEE Journal on Selected Areas in Communications*, vol. 37, no. 10, pp. 2184–2199, 2019.

[13] M. Soltani, V. Pourahmadi, A. Mirzaei, and H. Sheikhzadeh, "Deep learning-based channel estimation," *IEEE Communications Letters*, vol. 23, no. 4, pp. 652–655, 2019.

[14] M. Jankowski, D. Gündüz, and K. Mikolajczyk, "Airnet: Neural network transmission over the air," in *2022 IEEE International Symposium on Information Theory (ISIT)*, 2022, pp. 2451–2456.

[15] G. Liu, Z. Hu, L. Wang, J. Xue, H. Yin, and D. Gesbert, "Spatio-temporal neural network for channel prediction in massive MIMO-OFDM systems," *IEEE Transactions on Communications*, vol. 70, no. 12, pp. 8003–8016, 2022.

[16] J. Xia and D. Gündüz, "Meta-learning based beamforming design for miso downlink," in *2021 IEEE International Symposium on Information Theory (ISIT)*, 2021, pp. 2954–2959.

[17] J. Guo, C.-K. Wen, S. Jin, and G. Y. Li, "Overview of deep learning-based CSI feedback in massive MIMO systems," *IEEE Transactions on Communications*, vol. 70, no. 12, pp. 8017–8045, 2022.

[18] C. Wen, W. Shih, and S. Jin, "Deep learning for massive MIMO CSI feedback," *IEEE Wireless Communications Letters*, vol. 7, no. 5, pp. 748–751, 2018.

[19] J. Guo, C. Wen, S. Jin, and G. Y. Li, "Convolutional neural network-based multiple-rate compressive sensing for massive MIMO CSI feedback: Design, simulation, and analysis," *IEEE Transactions on Wireless Communications*, vol. 19, no. 4, pp. 2827–2840, 2020.

[20] Z. Lu, J. Wang, and J. Song, "Multi-resolution CSI feedback with deep learning in massive MIMO system," in *ICC 2020 - 2020 IEEE International Conference on Communications (ICC)*, 2020, pp. 1–6.

[21] Z. Hu, J. Guo, G. Liu, H. Zheng, and J. Xue, "MRFNet: A deep learning-based CSI feedback approach of massive MIMO systems," *IEEE Communications Letters*, vol. 25, no. 10, pp. 3310–3314, 2021.

[22] S. Tang, J. Xia, L. Fan, X. Lei, W. Xu, and A. Nallanathan, "Dilated convolution based CSI feedback compression for massive MIMO systems," *IEEE Transactions on Vehicular Technology*, vol. 71, no. 10, pp. 11 216–11 221, 2022.

[23] Y. Cui, A. Guo, and C. Song, "Transnet: Full attention network for CSI feedback in FDD massive MIMO system," *IEEE Wireless Communications Letters*, vol. 11, no. 5, pp. 903–907, 2022.

[24] H. Li, B. Zhang, H. Chang, X. Liang, and X. Gu, "CVLnet: A complex-valued lightweight network for CSI feedback," *IEEE Wireless Communications Letters*, vol. 11, no. 5, pp. 1092–1096, 2022.

[25] Y. Sun, W. Xu, L. Liang, N. Wang, G. Y. Li, and X. You, "A lightweight deep network for efficient CSI feedback in massive MIMO systems," *IEEE Wireless Communications Letters*, vol. 10, no. 8, pp. 1840–1844, 2021.

[26] Q. Yang, M. B. Mashhadi, and D. Gündüz, "Deep convolutional compression for massive MIMO CSI feedback," in *2019 IEEE 29th international workshop on machine learning for signal processing (MLSP)*. IEEE, 2019, pp. 1–6.

[27] M. B. Mashhadi, Q. Yang, and D. Gündüz, "Distributed deep convolutional compression for massive MIMO CSI feedback," *IEEE Transactions on Wireless Communications*, vol. 20, no. 4, pp. 2621–2633, 2021.

[28] B. Tolba, M. Elsabrouty, M. G. Abdu-Aguye, H. Gacanin, and H. M. Kasem, "Massive MIMO CSI feedback based on generative adversarial network," *IEEE Communications Letters*, vol. 24, no. 12, pp. 2805–2808, 2020.

[29] X. Chen, C. Deng, B. Zhou, H. Zhang, G. Yang, and S. Ma, "High-accuracy CSI feedback with super-resolution network for massive MIMO systems," *IEEE Wireless Communications Letters*, pp. 1–1, 2021.

[30] Z. Lu, X. Zhang, H. He, J. Wang, and J. Song, "Binarized aggregated network with quantization: Flexible deep learning deployment for CSI feedback in massive MIMO system," *IEEE Transactions on Wireless Communications*, pp. 1–1, 2022.

[31] Z. Zhang, Y. Zheng, C. Gan, and Q. Zhu, "Massive MIMO CSI reconstruction using CNN-LSTM and attention mechanism," *IET Communications*, vol. 14, no. 18, pp. 3089–3094, 2020.

[32] T. Wang, C.-K. Wen, S. Jin, and G. Y. Li, "Deep learning-based CSI feedback approach for time-varying massive MIMO channels," *IEEE Wireless Communications Letters*, vol. 8, no. 2, pp. 416–419, 2018.

[33] J. Jang, H. Lee, S. Hwang, H. Ren, and I. Lee, "Deep learning-based limited feedback designs for MIMO systems," *IEEE Wireless Communications Letters*, vol. 9, no. 4, pp. 558–561, 2020.

[34] F. Sohrabi, K. M. Attiah, and W. Yu, "Deep learning for distributed channel feedback and multiuser precoding in FDD massive MIMO," *IEEE Transactions on Wireless Communications*, vol. 20, no. 7, pp. 4044–4057, 2021.

[35] Z. Xu and J. Sun, "Model-driven deep-learning," *National Science Review*, vol. 5, no. 1, pp. 22–24, 2018.

[36] P. Wu, Z. Liu, and J. Cheng, "Compressed CSI feedback with learned measurement matrix for mmWave massive MIMO," *arXiv preprint arXiv:1903.02127*, 2019.

[37] Y. Wang, X. Chen, H. Yin, and W. Wang, "Learnable sparse transformation-based massive MIMO CSI recovery network," *IEEE Communications Letters*, vol. 24, no. 7, pp. 1468–1471, 2020.

[38] J. Guo, L. Wang, F. Li, and J. Xue, "CSI feedback with model-driven deep learning of massive MIMO systems," *IEEE Communications Letters*, vol. 26, no. 3, pp. 547–551, 2022.

[39] Z. Yin, W. Xu, R. Xie, S. Zhang, D. W. K. Ng, and X. You, "Deep CSI compression for massive MIMO: A self-information model-driven neural network," *IEEE Transactions on Wireless Communications*, vol. 21, no. 10, pp. 8872–8886, 2022.

[40] X. Liang, H. Chang, H. Li, X. Gu, and L. Zhang, "Changeable rate and novel quantization for CSI feedback based on deep learning," *IEEE Transactions on Wireless Communications*, vol. 21, no. 12, pp. 10 100–10 114, 2022.

[41] M. Nerini, V. Rizzello, M. Joham, W. Utschick, and B. Clerckx, "Machine learning-based CSI feedback with variable length in FDD

massive MIMO," *IEEE Transactions on Wireless Communications*, pp. 1–1, 2022.
[42] Z. Chen, Z. Zhang, Z. Xiao, Z. Yang, and K.-K. Wong, "Viewing channel as sequence rather than image: A 2-D seq2seq approach for efficient MIMO-OFDM CSI feedback," *IEEE Transactions on Wireless Communications*, pp. 1–1, 2023.
[43] R. Zhang and S. Li, "A proof of conjecture on restricted isometry property constants δ_{tk} $\left(0 < t < \frac{4}{3}\right)$," *IEEE Transactions on Information Theory*, vol. 64, no. 3, pp. 1699–1705, 2018.
[44] D. Meng and F. De La Torre, "Robust matrix factorization with unknown noise," in *Proceedings of the IEEE International Conference on Computer Vision*, 2013, pp. 1337–1344.
[45] D. Yang and J. Sun, "A model-driven deep dehazing approach by learning deep priors," *IEEE Access*, vol. 9, pp. 108 542–108 556, 2021.
[46] H. Wang, Q. Xie, Q. Zhao, and D. Meng, "A model-driven deep neural network for single image rain removal," in *2020 IEEE/CVF Conference on Computer Vision and Pattern Recognition (CVPR)*, 2020, pp. 3100–3109.
[47] 3GPP, "NR; Study on channel model for frequencies from 0.5 to 100 GHz," 2017, v14.1.0.
[48] T. L. Marzetta, "Noncooperative cellular wireless with unlimited numbers of base station antennas," *IEEE Transactions on Wireless Communications*, vol. 9, no. 11, pp. 3590–3600, 2010.
[49] X. Gao, O. Edfors, F. Rusek, and F. Tufvesson, "Massive MIMO performance evaluation based on measured propagation data," *IEEE Transactions on Wireless Communications*, vol. 14, no. 7, pp. 3899–3911, 2015.
[50] S. Payami and F. Tufvesson, "Channel measurements and analysis for very large array systems at 2.6 GHz," in *2012 6th European Conference on Antennas and Propagation (EUCAP)*, 2012, pp. 433–437.
[51] L. L. Magoarou, A. L. Calvez, and S. Paquelet, "Massive MIMO channel estimation taking into account spherical waves," in *2019 IEEE 20th International Workshop on Signal Processing Advances in Wireless Communications (SPAWC)*, 2019, pp. 1–5.
[52] H. Jiang, Z. Zhang, J. Dang, and L. Wu, "A novel 3-D massive MIMO channel model for vehicle-to-vehicle communication environments," *IEEE Transactions on Communications*, vol. 66, no. 1, pp. 79–90, 2018.
[53] Y. Chen and C. Han, "Deep CNN-based spherical-wave channel estimation for terahertz ultra-massive MIMO systems," in *GLOBECOM 2020 - 2020 IEEE Global Communications Conference*, 2020, pp. 1–6.
[54] S. Jaeckel, L. Raschkowski, K. Börner, and L. Thiele, "QuaDRiGa: A 3-D multi-cell channel model with time evolution for enabling virtual field trials," *IEEE Transactions on Antennas and Propagation*, vol. 62, no. 6, pp. 3242–3256, 2014.
[55] M. Fornasier and H. Rauhut, "Iterative thresholding algorithms," *Applied and Computational Harmonic Analysis*, vol. 25, no. 2, pp. 187–208, 2008. [Online]. Available: https://www.sciencedirect.com/science/article/pii/S1063520307001157
[56] I. O. Tolstikhin, N. Houlsby, A. Kolesnikov, L. Beyer, X. Zhai, T. Unterthiner, J. Yung, A. Steiner, D. Keysers, J. Uszkoreit *et al.*, "MLP-mixer: An all-MLP architecture for vision," *Advances in Neural Information Processing Systems*, vol. 34, 2021.
[57] D. P. Kingma and J. Ba, "ADAM: A method for stochastic optimization," *arXiv preprint arXiv:1412.6980*, 2014.
[58] Y. Bengio, N. Léonard, and A. Courville, "Estimating or propagating gradients through stochastic neurons for conditional computation," *arXiv preprint arXiv:1308.3432*, 2013.
[59] B. Jacob, S. Kligys, B. Chen, M. Zhu, M. Tang, A. Howard, H. Adam, and D. Kalenichenko, "Quantization and training of neural networks for efficient integer-arithmetic-only inference," in *Proceedings of the IEEE Conference on Computer Vision and Pattern Recognition*, 2018, pp. 2704–2713.
[60] Y. Bhalgat, J. Lee, M. Nagel, T. Blankevoort, and N. Kwak, "Lsq+: Improving low-bit quantization through learnable offsets and better initialization," in *Proceedings of the IEEE/CVF Conference on Computer Vision and Pattern Recognition Workshops*, 2020, pp. 696–697.
[61] S. K. Esser, J. L. McKinstry, D. Bablani, R. Appuswamy, and D. S. Modha, "Learned step size quantization," *arXiv preprint arXiv:1902.08153*, 2019.
[62] C. Finn, P. Abbeel, and S. Levine, "Model-agnostic meta-learning for fast adaptation of deep networks," in *International Conference on Machine Learning*, 2017, pp. 1126–1135.
[63] J. Guo, C.-K. Wen, M. Chen, and S. Jin, "Environment knowledge-aided massive MIMO feedback codebook enhancement using artificial intelligence," *IEEE Transactions on Communications*, vol. 70, no. 7, pp. 4527–4542, 2022.
[64] W. Utschick, V. Rizzello, M. Joham, Z. Ma, and L. Piazzi, "Learning the CSI recovery in FDD systems," *IEEE Transactions on Wireless Communications*, vol. 21, no. 8, pp. 6495–6507, 2022.

Zhengyang Hu received the B.S. degree in applied mathematics from Xi'an Jiaotong University, Xi'an, China, in 2019. He is currently working toward the Ph.D. degree in applied mathematics with Xi'an Jiaotong University, Xi'an, China. His current research interests include the deep learning for physical layer, massive MIMO and intelligent wireless communication.

Guanzhang Liu received the B.S. degree in applied mathematics from Harbin Engineering University, Harbin, China, in 2019. He is currently working toward the Ph.D. degree in applied mathematics with Xi'an Jiaotong University, Xi'an, China. His current research interests include the machine learning and intelligent wireless communication, time series analysis and prediction.

Jiang Xue received the B.S. degree in Information and Computing Science from the Xi'an Jiaotong University, Xi'an, China, in 2005, the M.S. degrees in Applied Mathematics from Lanzhou University, China and Uppsala University, Sweden, in 2008 and 2009, respectively. Prof. J. Xue received the Ph.D.degree in Electrical and Electronic Engineering from ECIT, the Queen's University of Belfast, U.K., in 2012. From 2013 to 2017, He was a Research Fellow with the University of Edinburgh, U.K.. Since 2017, Prof. J. Xue is with the National Engineering Laboratory for Big Data Analytics, Xi'an International Academy for Mathematics and Mathematical Technology, School of Mathematics and Statistics, Xi'an Jiaotong University, Pengcheng Lab, China, and he is supported by the 'Zhongying Young Scholars project'. His main interests include the machine learning and wireless communication, performance analysis of multiple antenna systems, CSI estimation and prediction and stochastic geometry.

Qi Xie received the B.Sc. and Ph.D degree from Xi'an Jiaotong University, Xi'an, China, in 2013 and 2020 respectively. He was a Visiting Scholar with Princeton University, Princeton, NJ, USA, from 2018 to 2019. He is currently an associate professor with School of Mathematics and Statistics, Xi'an Jiaotong University. His current research interests include model-based deep learning and filter parametrization-based deep learning.

Deyu Meng received the B.Sc., M.Sc., and Ph.D. degrees in 2001, 2004, and 2008, respectively, from Xi'an Jiaotong University, Xi'an, China. He is currently a professor with School of Mathematics and Statistics, Xi'an Jiaotong University, and adjunct professor with Faculty of Information Technology, The Macau University of Science and Technology. He currently serves as an associate editor of the IEEE Transactions on Pattern Recognition and Machine Intelligence, Science China- Information Sciences, and Frontiers of Computer Science. His current research interests include model-based deep learning, variational networks, and meta-learning.

Deniz Gündüz Deniz Gündüz [S'03-M'08-SM'13-F'22] received the B.S. degree in electrical and electronics engineering from METU, Turkey in 2002, and the M.S. and Ph.D. degrees in electrical engineering from NYU Tandon School of Engineering (formerly Polytechnic University) in 2004 and 2007, respectively. Currently, he is a Professor of Information Processing in the Electrical and Electronic Engineering Department at Imperial College London, UK, where he also serves as the deputy head of the Intelligent Systems and Networks Group. In the past, he held various positions at the University of Modena and Reggio Emilia (2019-22), University of Padova (2018, 2020), Centre Tecnologic de Telecomunicacions de Catalunya (CTTC) (2009-12), Princeton University (2007-09, 2009-11) and Stanford University (2007-09).

His research interests lie in the areas of communications and information theory, machine learning, and privacy. Dr. Gündüz is a Fellow of the IEEE, and a Distinguished Lecturer for the IEEE Information Theory Society (2020-22). He is an elected member of the IEEE Signal Processing Society Signal Processing for Communications and Networking (SPCOM) and Machine Learning for Signal Processing (MLSP) Technical Committees. He serves in editorial roles for the IEEE Transactions on Information Theory, IEEE Transactions on Communications and IEEE Transactions on Wireless Communications. He is the recipient of the IEEE Communications Society - Communication Theory Technical Committee (CTTC) Early Achievement Award in 2017, Starting (2016) and Consolidator (2022) and Proof-of-Concept (2023) Grants of the European Research Council (ERC), and several best paper awards.